www.czasopisma.pan.pl PAN POLSKA AKADEMIA NAUK www.journals.pan.pl

A R C H I V E S O F M E T A L L U R G Y A N D M A T E R I A L S

Volume 58 2013 Issue 1

DOI: 10.2478/v10172-012-0168-3

T. SADOWSKI*, T. BALAWENDER**, R. ŚLIWA**, P. GOLEWSKI*, M. KNEĆ*

MODERN HYBRID JOINTS IN AEROSPACE: MODELLING AND TESTING

NOWOCZESNE POŁĄCZENIA HYBRYDOWE W LOTNICTWIE: MODELOWANIE I BADANIA ESKPERYMENTALNE

The aim of the paper is to review different types of modern hybrid joints applied in aerospace. We focused on three particular cases: 1) spot welding – adhesive, 2) rivet-bonded and 3) clinch-bonded joints. The numerical models presented in the paper for these joints describe their complex behaviour under mechanical loading. The numerical calculations performed using ABAQUS code were compared to experimental results obtained by application of the Digital Image Correlation system (DIC) ARAMIS.

The results investigated within the paper lead to the following major conclusions:

- the strengthening of joints by application of adhesive significantly improve static strength,
- the final failure of the joined structural system significantly depends on the surface adhesive area,
- the stiffening effects of the hybrid joint lead to higher reliability and durability of the structural joints.

Keywords: clinching, hybrid joint, rivet-adhesive bonded joint, clinch – adhesive joint, spot welding – adhesive joint, FEA (finite element analysis), DIC (digital image correlation system)

W pracy dokonano przeglądu różnych typów połączeń hybrydowych stosowanych w lotnictwie. Szczególną uwagę zwrócono na trzy typy połączeń: 1) zgrzewanie punktowe – klejenie, 2) nitowanie – klejenie, 3) klinczowanie – klejenie. Modele numeryczne złączy zawarte w pracy, ujawniają złożoną i trudną do przewidzenia reakcję tych złączy na obciążenia mechaniczne. Obliczenia numeryczne porównano z wynikami eksperymentalnymi otrzymanymi za pomocą bezdotykowego systemu pomiaru odkształceń i naprężeń (DIC) ARAMIS.

Główne wnioski z prezentowanych badań:

- zastosowanie kleju powoduje istotne zwiększenie wytrzymałości statycznej testowanych połączeń,
- na końcowy efekt zniszczenia złącza hybrydowego znaczący wpływ ma powierzchnia złącza klejowego,
- zwiększona sztywność złączy hybrydowych powoduje, że mają one większą niezawodność i trwałość jako połączenia konstrukcyjne.

1. Introduction

The current manufacturers demands of modern structural parts of aircrafts requires application of new composite materials with different internal structure, specially introduced to the material, to modify its properties in order to get: excellent mechanical properties, lightweight, low cost and high security of structural elements creating whole airplanes. These applications are very important task in case of critical parts of the aircrafts as: elements of engines (e.g. turbine blades), wings, fuselage, joining of critical elements with various techniques etc. One of the idea of the new composites is to functionalize properties of the material in the form so called functionally graded materials – FGM (e.g. [1-5]) or by introduction layers between material components (e.g. [6-9]) or joined adherends (e.g. [10-15]) and as TBC covering turbine blades (e.g.[16-19]), etc. Application of adhesives with different nano-particles or carbon nano-tubes are other example to use of modern particle reinforced composites in aerospace technology (e.g. [20, 21]). This is the advantage of the idea to use combination of different phases in materials or joints to create new and stronger composite which guarantee higher durability and reliability of structural elements in aerospace.

The above ideas are the basis for improvements of joining technologies of structural parts in aerospace. Instead of using single joining technique as: riveting, spot welding, clinching or adhesive bonding a hybrid joining technique (e.g. [15, 22]) can be applied by combination of two simple ones, e.g.: riveted-bonding (e.g. [23, 24]), spot welded-bonding (e.g. [25, 26], clinched-bonding (e.g. [27-34]), etc. The first application of hybrid joints, one of them being adhesive bonding, was in a Russian aircraft construction from 1960 [27], and it was developed later on the Antonov AN-74 airplane, were a resistance spot welding was combined with the adhesive bonding.

In the paper we will review currently applied different hybrid joining techniques. The basic idea is to strengthen simple

* LUBLIN UNIVERSITY OF TECHNOLOGY, 20-618 LUBLIN, 40 NADBYSTRZYCKA STR., POLAND

** RZESZÓW UNIVERSITY OF TECHNOLOGY, 35-959 RZESZÓW, 8 POWSTANCÓW WARSZAWY STR., POLAND

joining technology by introduction additional adhesive layer between adherends, which have many positive effects, like: a higher static strength, improved fatigue strength, removing of sealing operations, better corrosion resistance.

The own experimental investigations done with: 1) rivet-adhesive bonded, 2) spot welding – adhesive and 3) clinch-adhesive bonded joints confirm the significant improvement of mechanical properties of hybrid joints in comparison to simple one.

The paper describes details of numerical model by application of FEA for proper characterisation of the mechanical response of these complex hybrid joints. The models incorporate description of the technological process of the joint creation (i.e. press forming of the clinch) as well as different aspects of damage processes which should be applied for full description of the degradation both: adhesive layers and adherends.

The received results lead to general conclusion that the hybrid joining significantly increases mechanical response of the joint, particularly as for load capacity.

2. Rivet-adhesive bonded joints

Let us consider the hybrid Double Lap Joints (DLJ) made of steel strips adhesive bond layer reinforced by a rivet. The rivet forming process introduces an initial compressive stress to the joint, making the hybrid joint non-symmetric in the thickness direction. The mechanical response of this DLJ was analysed in three steps: starting from a simple mechanical rivet joint, further – from a simple adhesive joint and finally – by analysis of the hybrid joint.

The experimental testing included the application of the 3-D Digital Image Correlation (DIC) system ARAMIS in order to monitor the displacements distribution during the joint testing up to final failure. A numerical modelling was performed by Finite Element Analysis (FEA) and software ABAQUS 6.6. It included the modelling of the riveting process, degradation of the adhesive layer by application of a Cohesive Zone Model (CZM) and fracture of the aluminium rivet, similar to [7]. The stress concentrations in different parts of the joint due to different reasons (riveting process, mechanical loading) were investigated.

2.1. Experimental tests

The samples were prepared from two different kinds of steel sheets with a Young's modulus equal to E_s = 210 GPa, and Poisson's ratio ν = 0.3. The steel used for the middle part of DLJ (3 mm thickness) was much stronger in comparison to that used for the 2 external thinner sheets (1.5 mm thickness).

The rivets, made of aluminium alloy having the Young's modulus equal to E_r = 70 GPa, whereas Poisson's ratio is equal to ν = 0.3. The mandrel was made of steel. The exerted force by the mandrel for the single rivet during forming process was equal to F_r = 2 kN.

The adhesive used for the DLJ was the heat curing epoxy adhesive Hysol 9514 (Loctite, Ireland). In order to get maximum tensile and shear strengths, the specimens were kept in the curing temperature 150°C for 30 min, according to producer recommendation. The shear strength was equal to τ^{max} = 45 MPa, whereas tensile strength σ^{max} = 44 MPa (data supplied by the manufacturer).

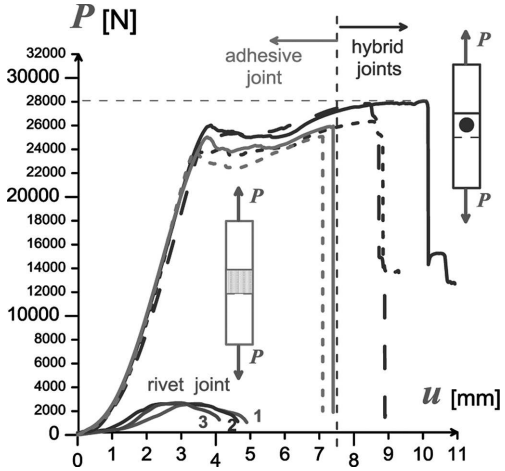

Fig. 1. Load-displacement curves for the riveted joints, the adhesive joints and the hybrid joints

The specimens were subjected to tensile loading using the ZWICK Z-100 testing machine at a crosshead displacement rate of 2 mm/min. Experimental results for the whole program with the three types of specimens are presented in Fig. 1. The steel parts joined mechanically by the rivet exhibit a relatively week strength. This is due to the fact that the rivet was made of aluminium alloy, having not high shear strength limit. The shape of the force-displacement diagram is in the first stage a linear behaviour, then yielding of steel strips takes place and finally crack propagation in the adhesive layers (after maximum load) in the most efforted zone of the joint started.

The adhesive joint with Hysol 9514 was extremely effective and tough, i.e. the strength of the joint is almost one order of magnitude higher in comparison to the rivet joints. The shape of the force-displacement curve is characteristic, i.e. after the first linear part, the curve reaches the local maximum at which the adhesive layers start to fail (damage initiation criterion is satisfied in the most efforted parts of the joint). Then, the bonding area load starts to reduce. Therefore, one can observe a local small decrease of the force and then stabilisation corresponding to further gradual development of failure zones in adhesive layers, followed by almost linear increase up to the maximum load.

The hybrid joints have the same geometry as the simple joints. The adhesive was applied on the cleaned steel adherends and then the joint was reinforced by a simple rivet. The whole joint was cured at 150°C for 30 min. The averaged thickness of the adhesive, measured on the specimen, was equal to 0.2 mm. The force-displacement curves of the hybrid joints are similar to those of the adhesive joints. However, one can observe an increase of the failure load due to the presence of the rivet and synergy between the adhesive and the rivet. Moreover, a significant increase of the displacement at failure is observed for the hybrid joint. Failure takes place at the two bonding interfaces and the rivet.

2.2. Numerical model

3D finite element model was created in order to investigate numerically the 3 types of joint behaviour. The following types of elements were applied to the analysis: 8 node brick elements with reduced integration for modelling the steel adherends response, 4 node tetrahedral elements were used for the rivet modelling and 8-node three-dimensional cohesive elements for the adhesive layer. The analyses were done with the explicit version of the ABAQUS finite element code using arbitrary Lagrangian-Eulerian adaptive meshing.

Rivet forming process was modelled introducing the contact between the adherends, the rivet and the mandrel, i.e. the general contact algorithm in ABAQUS/Explicit was used with edge-to-edge contact penetrations. The contact properties were assumed as a "hard" contact in the normal direction without friction. One can observe the high plastic stress concentrations in the regions surrounding the penetration of the rivet by the mandrel. In this way, a compressive state is introduced in the joint, which significantly improves the load capacity of the whole joint. The permanent state of stress and strain created during the riveting process constitutes the initial stage for further analysis of the DLJ behaviour.

To simulate gradual decohesion and the failure process of the adhesive layer, a cohesive zone model CZM was applied in FEA calculations, e.g. [35 - 39]. For the analysis of degradation process the following damage initiation criterion which depend on current state of stress $\{\sigma_n, \sigma_t, \sigma_s\}$ was applied:

$$\left(\frac{\sigma_n}{\sigma_n^{\max}}\right)^2 + \left(\frac{\sigma_t}{\sigma_t^{\max}}\right)^2 + \left(\frac{\sigma_s}{\sigma_s^{\max}}\right)^2 = 1, \qquad (1)$$

where σ_n is the normal stress to the surface of the adhesive layer, whereas σ_t and σ_s are the shear stress components along the adhesive layer. For the considered adhesive Hysol 9514 ($\sigma_n^{\max} = 44$ MPa $\approx \sigma_t^{\max} = \sigma_s^{\max} = 45$ MPa) one can assume that the damage initiation process can be treated as isotropic.

The damage evolution criterion in the most general case is formulated as a power law and depends on the fracture energy in the three considered modes: normal $n = I$and two tangential:$t = II$, $s = III$:

$$\left(\frac{G_I}{G_{Ic}}\right)^2 + \left(\frac{G_{II}}{G_{IIc}}\right)^2 + \left(\frac{G_{III}}{G_{IIIc}}\right)^2 = 1 \qquad (2)$$

where $G_{Ic}, G_{IIc}, G_{IIIc}$ are the critical values of the fracture energies (e.g. [40 – 43]). The fracture energy, measured by DCB test, is equal to $G_{Ic} = 905$ J/m^2. Due to lack of experimental data, it was assumed that $G_{IIc} = G_{IIIc} = G_{Ic}$, i.e. the failure of the cohesive layer is isotropic. In simulation we assumed that the total damage of a finite element of the adhesive layers is reached, when the fracture energy criterion (2) is satisfied. Then the finite element was removed from the mesh.

Figure 2 presents the Huber – von Mises stress concentration at the stage before final failure of the adhesive joint. The major part of the adhesive layers area is damaged in the FEA model. However, the central parts are still strong enough to transmit the load. One can observe the progression of the failure zone in the adhesive layers due to:

- significant development of plastic strains in the steel adherends (from the loading force side);
- total unloading at the ends of the adherents (full decohesion of joined parts).

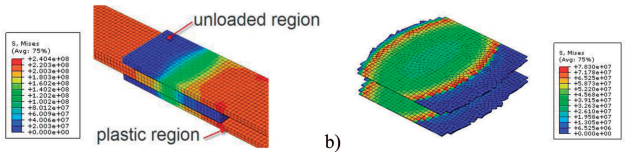

Fig. 2. Stress distribution in the adherends a) and degradation state of the adhesive layer b) in the final failure stage of the adhesive joint (in [Pa])

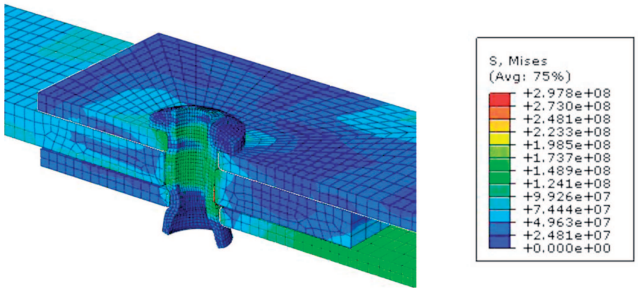

Fig. 3. Stress distribution during the rivet shearing in the hybrid joint (in [Pa])

Figure 3 shows distribution of the Huber – von Mises stress in the final stage of degradation process of the hybrid joint. After total decohesion of the adhesive layers shearing rivet process initiates and leads to final failure.

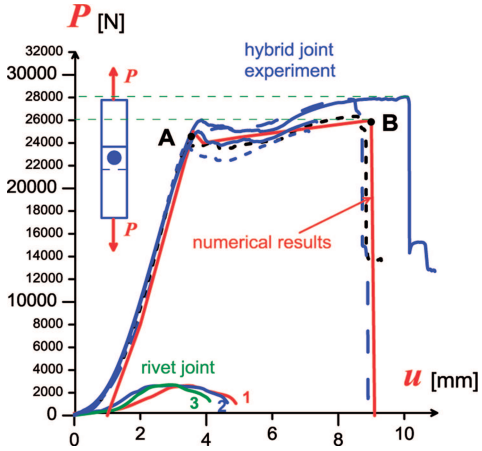

Fig. 4. Comparison of experimental results and numerical simulation

Figure 4 presents a comparison of experimental results and numerical simulation. The shape of the force-displacement curve is similar to purely adhesive joint, but the failure load was increased by the rivet. At point A, the gradual degradation process starts in the adhesive layers, whereas at point B the total capacity of adhesive layers is reached and the shearing of the rivet takes place.

3. Spot welding – adhesive joints

The second type of joining is spot welding-adhesive joint made of aluminium 2024 sheet of the thickness 0.6 mm – typical alloys for making fuselage of small aircrafts, Fig. 5. The characteristic values of the material are: the Young's modulus was equal to $E_{al} = 70$ GPa, $\nu = 0.3$, $R_m = 330$ MPa.

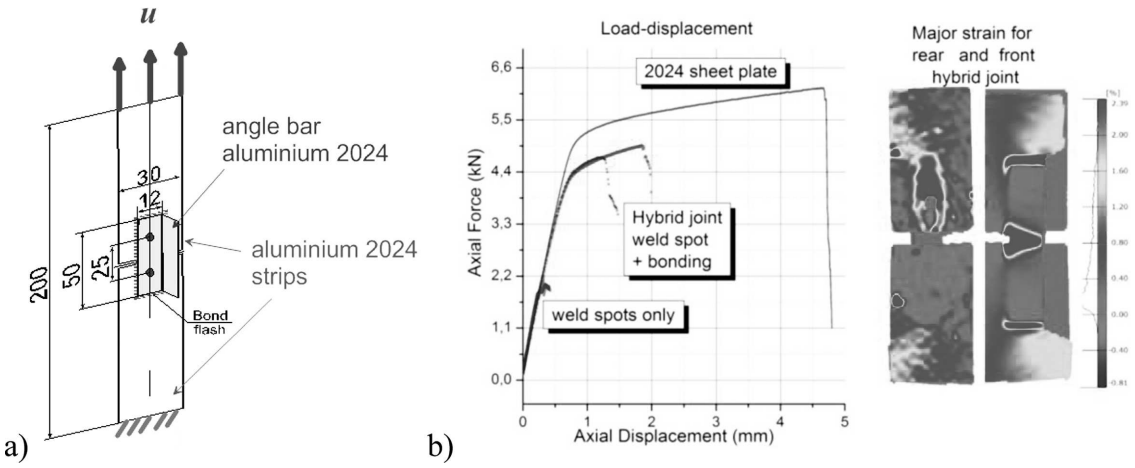

Fig. 5. a) Specimen dimensions, b) experimental load-displacement curve with corresponding DIC strain distribution

The adhesive used for samples preparation was two component epoxy CHS-EPODUR 619 (Spolchenie, Czech Republik). This is modified liquid epoxy resin with the low dynamic viscosity coefficient equal to 0.8 Pas. The shear strength was equal to $\tau^{\max} = 24.4$ MPa and $\sigma^{\max} = 24.4$ MPa. The Young's modulus was equal to $E_{ad} = 2$ GPa, whereas $G_{ad} = 0.8$ GPa and $\nu = 0.3$.

The weld-bonded joints were produced by the weld-through technique. This process was performed in order to create spots located in the middle part of the laps (of the area 12 mm × 25 mm), Fig. 5a). The diameter of the nuggets for the considered joint was 6 mm.

In the final stage of the hybrid joint technological process the low-viscosity adhesive is introduced between joint faying surfaces by capillary action to fulfil the overlap area of the joint. The curing procedure was the following: 24 hours in 23°C and then 4 hours in 140°C.

3.1. Experimental tests

The specimens were subjected to tensile loading using the MTS testing machine (100 kN) with displacement rate equal to 2 mm/min. Because of very complex specimen shape in order to monitor the whole displacement process two ARAMIS sensors were simultaneously used from both specimen sides.

Figure 5b) shows load-displacement curves for all tested kinds of joints and corresponding DIC major strains distribution. The obtained results indicate that the deformation process of the real joint is highly non-homogeneous, anisotropic and non-uniform. The load-displacement diagram indicates that simple spot welded joint for the considered sample geometry exhibits a relatively weak strength. The maximum force P_{max} is equal to 1.8 kN and corresponds to the fracture force of the single spot. The carrying load is just concentrated in the small cross section of the 2 spots. For the hybrid joint at the load level 4.4 kN the change of the angle of inclination takes place. At this stage of deformation a visible adhesive layer degradation process starts, i.e. the overlap area of the adhesive carrying load decreases. The load increase leads to destruction of the adhesive layer up to the maximum force P_{max}. Then sudden drop of the carrying force begins and the final failure of the hybrid joint takes place.

The hybrid joint has almost 2.5 times higher load capacity in comparison to the simple weld spot joint.

3.2. Numerical results

The numerical model was created with application fasteners technique to simple spot joints and ABAQUS code. The adhesive layer with thickness 0,1 mm was modelled by application cohesive elements. The fracture energy of the adhesive , measured by DCB test, was equal to $G_{cr} = 750$ J/m^2. In the numerical analysis both criteria (1) and (2) were included.

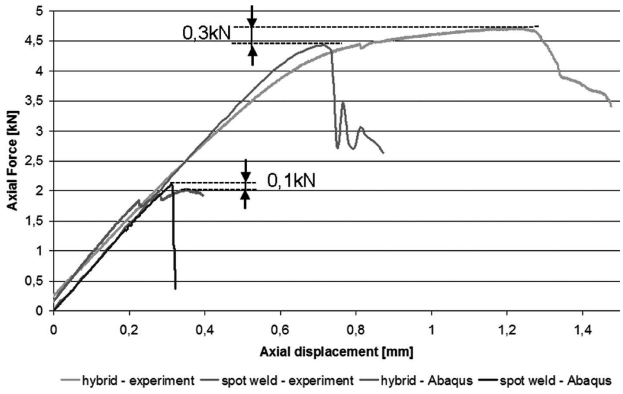

Fig. 6. Force-displacement diagram; comparison of experimental and numerical results

Figure 6 presents numerical results. In case of the pure spot weld joint, the difference between maximum force P_{max} obtained from the experiment and the ABAQUS program was equal to 0.1 kN. This is about 4.5% of the experimental force. Furthermore, the maximum force for both results, i.e. numerical and experimental one, took place almost at the same displacements. For the hybrid joint we also received convergence of results concerning P_{max} at the level of 6.3%. However, there is divergence for displacement at which the failure of the joint initiates. For the numerical simulation this characteristic is about 0.7 mm while in real sample after testing 1.25 mm. That big difference is caused by the high gradient of plastic deformation and further gradual rupture of material in the surrounding area of the spot weld. The concentrated large deformations cause additional displacement before the final fail-

ure, what was reflected in the experimental force-displacement diagram.

4. Clinch-bonded joints

Clinching is a mechanical joining technique for point joining of sheet metals without the use of any additional elements (e.g. [28, 29, 44, 45]). With clinching, the sheets are squeezed between a punch and a die, forming a shape that locks the sheets together. The strength of the joint is not high in comparison with other joining methods. Combining clinching with adhesive bonding can increase the joint strength and create a hybrid joining method with new potential applications in the manufacturing industry [31-34]. The paper presents results of experimental and numerical testing of such clinch-bonded joints. Up till now there is no discussion in the literature of the sequence of technological operations in manufacturing of the hybrid joints, i.e. investigations of the effect of clinching before and after curing of the adhesive.

4.1. Experimental tests

The experimental investigations of the clinched joints were realized in the pull tests of lap joints. The clinch lap joints were manufactured by the tool set presented in previous publications [33, 34]. ETP-copper and low carbon steel sheets were used to prepare the test specimens, which were composed of two strips (~132×35×1 mm) joined with 35 mm overlap length. Adhesive used in the bonded and hybrid (clinched and bonded) specimens preparation, was Pattex® Repair Epoxy, a commercial product of Henkel AG &Co.KGaA.

Two methodologies of hybrid specimen were applied: 1 – adhesive curing before clinching and 2 – clinching before adhesive curing. The results obtained for these both methods are shown in Fig. 7. Although, big differences in geometrical parameters between clinched and hybrid specimens were not observed, the essential increase in their mechanical properties was noticed, i.e. force and energy absorption, e.g. [31, 33, 34].

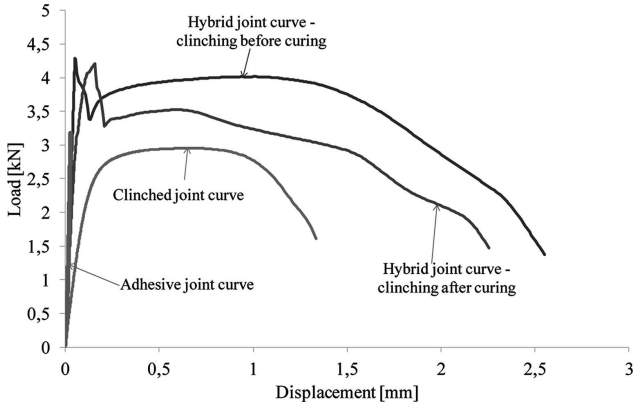

Fig. 7. Experimental load–displacement curves obtained for adhesive, clinched and hybrid joints

The hybrid joint – clinching before adhesive curing disclose more rigidity and greater bearing load than the hybrid joint – clinching after curing, as it can be observed in diagrams presented in Fig 7. This result is particularly visible in the second stage of the hybrid joint curves, when the adhesive bonds are destroyed (after maximal load point) and the load is borne by the clinch joint.

4.2. Numerical results

Numerical simulations were performed using ABAQUS software with dynamic explicit approach. The blanks were meshed using C3D8R elements, involving in 10816 elements for each blank and four elements in thickness direction. The assumptions made in simulation process are shown in Table 1 and the simulation results are shown in Fig 8. The quadratic stress-based damage initiation criterion CSQUADSCRT for cohesive surfaces in general contact was used to estimate damage of the adhesive layer; damage initiation occurs when the stresses satisfy the specified quadratic nominal stress criterion given by:

$$\left(\frac{t_n}{t_n^0}\right)^2 + \left(\frac{t_s}{t_s^0}\right)^2 + \left(\frac{t_t}{t_t^0}\right)^2 = 1, \tag{3}$$

where t_n^0, t_s^0, t_t^0 are the peak values of the nominal stress when the deformation is either purely normal to the interface or purely in the first or the second shear direction respectively. The adhesive layer parameters were assumed as: E =3000MPa, $t_n^0 = t_s^0 = t_t^0 = 6$ MPa, fracture energy was equal to $G_{Ic} = 275$ J/m^2 (measured by DCB test).

TABLE 1

Contact conditions in the clinched joint cavity

Simulated stages of the process	Clinching before curing of adhesive (A simulation)	Clinching after curing of adhesive (B simulation)
Sheet drawing	Lack of friction between joined sheets; lack of cohesion properties	There are cohesion properties- friction 0.1 on the contact surfaces after adhesive layer failure
Anneal	Deletion of drawing stresses –it is in real process, when clamping the joint	No deletion of drawing stresses
Opening the clinching tools	Engaging of cohesion properties and then friction 0.1 on the contact surfaces after adhesive layer failure	No changes. Friction 0.1 on the contact surfaces
Joint failure	No changes in the contact definition	No changes in the contact definition

Table 1 describes assumptions in the numerical modelling of the clinch-bonded joints at different stages of their manufacturing starting from the sheet drawing up to the final failure.

Differences between experimental and numerical simulations are in the shearing force value. The experimental force values obtained in the pull test were in the range 4÷4.5 kN, whereas the simulation results were 5÷7 kN. In experiments, greater force values were obtained for hybrid specimens prepared by procedure clinching before curing; inverse results were obtained in simulation.

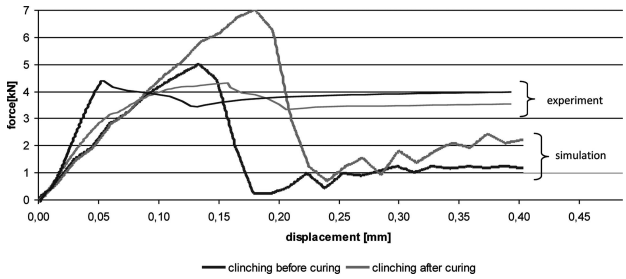

Fig. 8. Simulated separation force evolution in the pull test - comparison between: clinching before curing and clinching after curing

The main reason of the discrepancy between experiment and simulation results, concerning hybrid specimen procedures (clinching before and after adhesive curing), are numerical simulation assumptions, but it should be noticed, that the differences between experimental results, obtained in these two applied procedures, are small. So, it is difficult to establish simulation conditions satisfying exactly experiment requirements. The presented simulation is only a trial of possible simulations by FEM, but the simulation assumptions should be discussed and corrected in future investigations.

5. Conclusions

The results investigated within the paper lead to the following major conclusions:

- the strengthening of simple joints (clinching, riveting and spot welding) by application of adhesive significantly improve static strength,
- the increase of the load capacity of the rivet – adhesive hybrid joint in comparison to purely riveted one is higher more than 10 times. In comparison to simple adhesive bond this difference is approximately equal to 10%. However, energy consumed by the specimen to the final failure is several times higher in case of the hybrid joints,
- the spot welded – adhesive hybrid joint has almost 2.5 times higher load capacity in comparison to the simple weld spot joint,
- the greater force values were obtained for hybrid specimens prepared by clinching before curing,
- the final failure of the hybrid joined structural system significantly depends on the type of the applied adhesive during specimen manufacturing and the surface adhesive area. The high fracture properties of the adhesive layer can significantly influence the level of loading capacity and increase the energy absorbtion capacity up to the final failure,
- the stiffening effects of the hybrid joint lead to higher reliability and durability of the structural joints.

Acknowledgements

Financial support from Structural Funds in the **Operational Programme – Innovative Economy (IE OP, Poland)** financed from the European Regional Development Fund – Project "Modern material technologies in aerospace industry", No POIG.0101.02-00-015/08 is gratefully acknowledged (RT-15: Unconventional technologies of joining elements of aeronautical constructions).

This work was financially supported by Ministry of Science and Higher Education within the statutory research number S/20/2013.

REFERENCES

[1] T. Sadowski, M. Boniecki, Z. Librant, K. Nakonieczny, Theoretical prediction and experimental verification of temperature distribution in FGM cylindrical plates subjected to thermal shock. Int. J. Heat and Mass Transfer **50**, 4461-4467 (2007).

[2] T. Sadowski, S. Ataya, K. Nakonieczny, Thermal analysis of layered FGM cylindrical plates subjected to sudden cooling process at one side – comparison of two applied methods for problem solution, Comp. Mater. Sci. **45**, 624-632 (2009).

[3] T. Sadowski, A. Neubrand, Estimation of the crack length after thermal shock in FGM strip, Int. J. Fract. **127**, 135-140 (2004).

[4] K. Nakonieczny, T. Sadowski, Modelling of thermal shock in composite material using a meshfree FEM, Comp. Mater. Sci. **44**, 1307-1311 (2009).

[5] T. Sadowski, K. Nakonieczny, Thermal shock response of FGM cylindrical plates with various grading patterns, Comput. Mat. Sci. **43**, 171-178 (2008).

[6] T. Sadowski, S. Hardy, E. Postek, Prediction of the mechanical response of polycrystalline ceramics containing metallic inter-granular layers under uniaxial tension. Comput. Mat. Sci. **34**, 46-63 (2005).

[7] T. Sadowski, S. Hardy, E. Postek, A new model for the time-dependent behaviour of polycrystalline ceramic materials with metallic inter-granular layers under tension. Mat. Sci. Eng. A **424**, 230-238 (2006).

[8] T. Sadowski, E. Postek, Ch. Denis, Stress distribution due to discontinuities in polycrystalline ceramics containing metallic inter-granular layers. Comput. Mat. Sci. **39**, 230-236 (2007).

[9] T. Sadowski, T. Nowicki, Numerical investigation of local mechanical properties of WC/Co composite, Comput. Mat. Sci. **43**, 235-241 (2008).

[10] L.F.M. da Silva, P.J.C. das Neves, R.D. Adams, J.K. Spelt, Analytical models of adhesively bonded joints – Part I: Literature survey, Int. J. Adhes. & Adhes. **29**, 319-330 (2009).

[11] L.F.M. da Silva, P.J.C. das Neves, R.D. Adams, J.K. Spelt, Analytical models of adhesively bonded joints – Part II: Comparative study, Int. J. Adhes. & Adhes. **29**, 331-341 (2009).

[12] A.V. Pocius, Adhesion and adhesives technology, Hasner, New York (1997).

[13] R.D. Adams, J. Comyn, W.C. Wake, Structural adhesive joints in engineering. 2nd ed. Chapman&Hall, London (1997).

[14] L.F.M. da Silva, A. Öchsner (Eds), Modelling of adhesively bonded joints, Springer (2008).

[15] L.F.M. da Silva, A. Öchsner, R.D. Adams, Handbook of Adhesion Technology, Springer (2011).

[16] T. Sadowski, P. Golewski, Multidisciplinary analysis of the operational temperature increase of turbine blades in combustion engines by application of the ceramic thermal barrier coatings (TBC), Comp. Mater. Sci. **50**, 1326-1335 (2011).

[17] T. Sadowski, P. Golewski, The influence of quantity and distribution of cooling channels of turbine elements on level of stresses in the protective layer TBC and the efficiency of cooling, Comp. Mater. Sci. **52**, 293-297 (2012).

[18] T. Sadowski, P. Golewski, Detection and numerical analysis of the most efforted places in turbine blades under real working conditions, Comp. Mater. Sci. **64**, 285-288 (2012).

[19] T. Sadowski, P. Golewski, The analysis of heat transfer and thermal stresses in thermal barrier coatings under exploitation, Defect and Diffusion Forum **326-328**, 530-535 (2012).
[20] Z. Wu, J. Li, D. Timmer, K. Lorenzo, S. Bose, Study of processing variables on the electrical resistivity of conductive adhesives, Int. J. Adhes. & Adhes. **29**, 488-494 (2009).
[21] H. Zhao, T. Liang, B. Liu, Synthesis and properties of copper conductive adhesives modified by SiO_2 nanoparticles, Int. J. Adhes. & Adhes. **27**, 429-433 (2007).
[22] L.F.M. da Silva, A. Öchsner, A. Pirondi (Eds), Hybrid adhesive joints, Springer (2011).
[23] T. Sadowski, M. Kneć, P. Golewski, Experimental investigations and numerical modelling of steel adhesive joints reinforced by rivets, Int. J. Adh&Adhes **30**, 338-346 (2010).
[24] T. Sadowski, P. Golewski, E. Zarzeka-Raczkowska, Damage and failure processes of hybrid joints: adhesive bonded aluminium plates reinforced by rivets, Comp. Mater. Sci. **50**, 1256-1262 (2011).
[25] S.M.H. Darwish, Science of weld-adhesive joints, in da Silva, L.F.M., Pirondi, A., Öchsner A. (Eds), Hybrid adhesive joints, (Springer, 2011) p. 1-36.
[26] T. Sadowski, M. Kneć, P. Golewski, Spot welding-adhesive joints: modelling and testing, J. Adhesion, (under review).
[27] A. Pirondi, F. Moroni, Science of Clinch–Adhesive Joints, in Hybrid adhesive joints. Advanced Structured Materials, Volume 6, Springer 2011, L.F.M. da Silva, A. Pirondi, A. Öschner (Eds), pp. 109-147.
[28] J. Varis, Ensuring the integrity in clinching process. J. Mater. Proc. Technol. **174**, 277-285 (2006).
[29] J. Varis, J. Lepistö, A simple testing-based procedure and simulation of the clinching process using finite element analysis for establishing clinching parameters. Thin Walled Struct. **41**, 691-709 (2003).
[30] M. Oudjenea, L. Ben-Ayed, On the parametrical study of clinch joining of metallic sheets using the Taguchi method, Engineering Structures **30**, 1782-1788 (2008).
[31] T. Sadowski, T. Balawender, Technology of Clinch – Adhesive Joints, in Hybrid adhesive joints. Advanced Structured Materials, Volume 6, Springer 2011, L. F. M. da Silva, A. Pirondi, A. Öschner (Eds), pp. 149-176.
[32] F. Moroni, A. Pirondi, F. Kleiner, Experimental analysis and comparison of the strength of simple and hybrid structural joints, Int. J. Adh&Adhes **30**, 367-379 (2010).
[33] T. Balawender, T. Sadowski, Experimental and numerical analyses of clinched and adhesively bonded hybrid joints, J. Adhes. Sci Technol. **25**, 2391-2407 (2011).
[34] T. Balawender, T. Sadowski, M. Kneć, Technological problems and experimental investigation of hybrid: clinched – adhesively bonded joint, Arch. Metall. Mat. **56**, 439-446 (2011).
[35] A. Needleman, A continuum model for void nucleation by inclusion debonding, J. Appl. Mech. **54**, 525-531 (1987).
[36] V. Tvergaard, J. Hutchinson, The relation between crack growth resistance and fracture process parameters in elastic-plastic solids, J. Mech. Phys. Solids **40**, 1377-1397 (1992).
[37] E. Postek, T. Sadowski, Assessing the Influence of Porosity in the Deformation of Metal-Ceramic Composites, Composite Interfaces **18**, 57-76 (2011).
[38] V. Burlayenko, T. Sadowski, Influence of skin/core debonding on free vibration behaviour of foam and honeycomb cored sandwich plates, Int. J. Non-Linear Mechanics **45**, 959-968 (2010).
[39] V. Burlayenko, T. Sadowski, Analysis of structural performance of aluminium sandwich plates with foam-filled hexagonal foam, Comp. Mater. Sci. **45**, 658-662 (2009).
[40] L. Marsavina, T. Sadowski, Fracture parameters at bi-material ceramic interfaces under bi-axial state of stress. Comp. Mater. Sci. **45**, 693-697 (2009).
[41] T. Sadowski, L. Marsavina, N. Peride, E.-M. Craciun, Cracks propagation and interaction in an orthotropic elastic material: analytical and numerical methods, Comput. Mat. Sci. **46**, 687-693 (2009).
[42] L. Marsavina, T. Sadowski, Kinked cracks at a bi-material ceramic interface – numerical determination of fracture parameters. Comput. Mat. Sci. **44**, 941-950 (2009).
[43] T. Sadowski, G. Golewski, Effect of aggregate kind and graining on modelling of plain concrete under compression, Comput. Mat. Sci. **43**, 119-126 (2008).
[44] T.A. Barnes, I.R. Pashby, Joining techniques for aluminium spaceframes used in automobiles. Part II – adhesive bonding and mechanical fasteners. J. Mater. Proc. Technol. **99**, 72-79 (2000).
[45] H.P. Liebig, J. Bober, R. Beyer, Connecting sheet metal by press joining. Bänder Bleche Rohre **25**(9), 7 (1984). Vogel-Verlag, Würzburg

Received: 20 April 2012.